High-pressure mesomorphic behavior of a chiral polyacrylate by x-ray diffraction *in situ*

O. Francescangeli,[1] C. Ferrero,[2] M. Lorenzen,[2] P. Bösecke,[2] B. Paci,[1] and R. Caciuffo[1]
[1]*Dipartimento di Scienze dei Materiali e della Terra and Istituto Nazionale per la Fisica della Materia, Università di Ancona, Via Brecce Bianche, I-60131 Ancona, Italy*
[2]*European Synchrotron Radiation Facility, Boîte Postale 220, F-38043 Grenoble Cedex, France*
(Received 20 January 1997)

The high-pressure mesomorphic behavior of a chiral liquid crystalline polyacrylate has been studied by x-ray diffraction *in situ*. The results show the existence of monolayer smectic-A^* and bilayer smectic-C^* mesophases that coexist in the thermally untreated sample over a well-defined range of temperatures, from ambient pressure up to 133 MPa. Hydrostatic pressures of the order of 100–220 MPa are found to affect strongly the polymorphic behavior of the sample. The smectic-A^* mesophase, which at ambient pressure coexists with an interdigitated smectic-C^* structure, is stabilized over a temperature range which increases with pressure, whereas the formation of the smectic-C^* phase is inhibited above 220 MPa. The pressure increment is found to introduce static positional disorder, and to reduce the long-range positional order in the smectic structure strongly. A transition sequence from the isotropic melt through the smectic-A^* phase to a new crystalline structure is found by cooling isobarically down to room temperature. The proposed pressure-temperature phase diagram suggests the occurrence of peculiar disorder-order-disorder transitions as pressure is reduced isothermally. [S1063-651X(97)12606-X]

PACS number(s): 61.30.Eb, 61.10.Eq

I. INTRODUCTION

Chiral smectic liquid crystals containing biphenylene units are currently the focus of major interest in material science [1–4]. These polymers can form chiral smectic-C^* phases with optimal ferroelectric and nonlinear optical characteristics comparable to those of their low-molecular counterparts. In addition, it has been shown [5] that they can exhibit chiral smectic-A^* phases with electroclinic properties [6]. The ferroelectric properties of the chiral smectic-C^* mesophase and the peculiar electroclinic response of the chiral smectic-A^* phase have shown great potential in a variety of electro-optic applications [7–9]. These findings have stimulated further investigation into the synthesis and properties of chiral smectic polymers containing the biphenyle core [10].

In recent papers [11,12] it has been reported the synthesis and the liquid crystal behavior of the chiral polyacrylate 1, based on the biphenyl mesogenic moiety spaced from the backbone by a heptamethylene spacer and substituted in the 4-position by a methylbutoxy group.

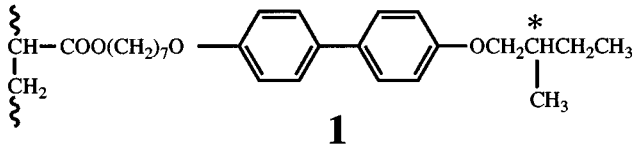

1

This polymer is one member of a family of side-chain polyacrylates consisting of variously spaced and substituted biphenilene units [13]. The x-ray-diffraction patterns at ambient pressure showed the existence of monolayer smectic-A^* and bilayer smectic-C^* mesophases which coexisted over a well-defined range of temperature. The high thermal stability of the mesogenic unit combined with the relatively low transition temperatures of polyacrylate 1 prevented microstructural rearrangements and degradation processes in the molten state which made the polymer promising for technological applications.

This paper reports the results of a high-pressure x-ray-diffraction study of polyacrylate 1 performed in order to determine the modifications induced by an external pressure to the mesomorphic behavior as a consequence of the reduced molar volume. The study of pressure-induced structural modifications in liquid crystalline (LC) polymers is a field of research essentially unexplored, and only few reports are available in the literature concerning this topic [14–18]. In the mesophases of LC polymers, the mesogenic and polymeric properties are closely coupled, and the macromolecular packing arises from a critical interplay between the ordering propensity, as imparted by anisotropic interactions among the mesogenic groups, and the chain constraints dictated by the configurational characteristics. In principle these latter should be strongly affected by pressure as a consequence of the variation of the molar volume. Apart from the fundamental interest, these studies are also interesting from an applicative point of view, since they allow one to explore the possibility of extending the interval of thermal stability of the chiral smectic mesophases, in particular up to room temperature, by submitting the material to an external pressure. This possibility seems to be promising since high-pressure treatment does not necessarily imply a complication in the material processing, as high pressures are routinely used in polymer industry.

The pressure-temperature phase diagram of polyacrylate 1, derived on the basis of the experimental observations, highlights the strong influence of hydrostatic pressures of the order of 100–220 MPa on the polymorphic behavior of the polymer. In particular, it shows that a pressure-induced stabilization of the chiral smectic-A^* phase of the polyacrylate can be achieved, and suggests the occurrence of a peculiar disorder-order-disorder transition as pressure is reduced iso-

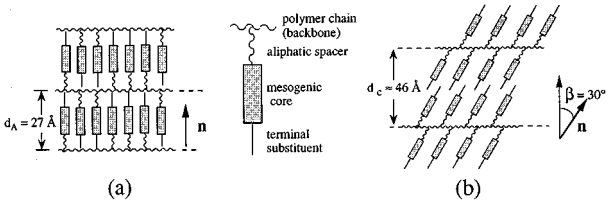

FIG. 1. Schematic representation of the macromolecular arrangement (a) in the S_{A*1} and (b) S_{C*2} mesophases.

thermically. The former effect was reported in a previous paper [14]. The pressure effects on the smectic ordering are quantitatively evaluated in terms of the modification of both the electron density profile along the normal to the smectic layers, and the positional smectic order parameters.

II. EXPERIMENTAL DETAILS

The experiment was carried out by using the small-angle x-ray scattering camera of the high brilliance beamline [19] at the European Synchrotron Radiation Facility, Grenoble, France, equipped with a high pressure cell which can operate up to 1 GPa at temperatures up to 570 K [19]. This cell consists of a cylinder of hardened maraging steel with a perpendicular bore for the x-ray windows. Pressure is produced by a piston driven by a hydraulic oil pump through a mechanical amplifier. Heating is provided by an external coil, and the temperature at the sample position is measured by a standard thermocouple placed outside the pressurized region, short below the sample position. Measurements were performed on a 3-mm-thick powder sample at two different pressures (133 and 220 MPa), in the temperature range between 300 and 500 K; the highest temperature in all cases being above the clearing point of the sample. The wavelength of the incident beam was $\lambda=0.0763$ nm and the q range explored varied between 0.63 and 5.03 nm^{-1} ($q=4\pi \sin\theta/\lambda$).

III. RESULTS AND DISCUSSION

A. Mesomorphic behavior at 133 MPa

A detailed description of the mesomorphic behavior of the sample at atmospheric pressure was reported in a previous paper [11]. On cooling down from the isotropic liquid, two different disordered smectic structures, namely, a bilayer smectic-C^* (S_{C*2}) and a monolayer smectic-A^* (S_{A*1}), coexist in the temperature range between the isotropization point ($T=406$ K) and $T=373$ K. However, the S_{A*1} phase occupies a volume fraction which becomes progressively smaller as the temperature is reduced, and finally disappears at about 373 K. Below this temperature, the S_{C*2} mesophase is stable, down to room temperature where no crystallization is observed even after prolonged annealing. The S_{A*1} mesophase is not observed in the first heating of a thermally untreated sample, but it appears above 373 K in all the thermal cycles following isotropization, which highlights the enantiotropic nature of this phase. A schematic picture of the macromolecular organization in the two mesophases is shown in Fig. 1. The electron density profile $\rho(z)$ along the normal to the smectic layers in the smectic-C^* mesophase, deduced from the experimental diffraction pattern, indicated the presence of a minor interdigitation of the terminal substituents, thus indicating that the configuration of the side chains does not depart considerably from the fully extended one. In agreement with this, the high values of the positional smectic order layer parameters calculated for the first five harmonics of the positional distribution function suggested a well-ordered layer structure.

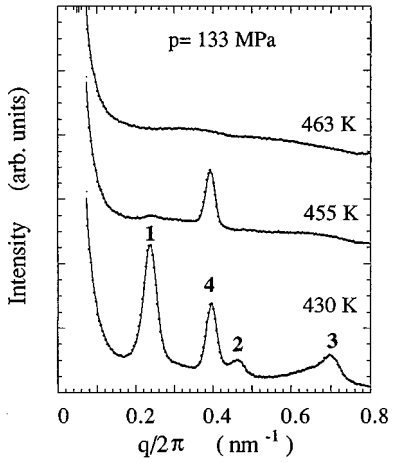

FIG. 2. Selected x-ray-diffraction patterns obtained during the first heating cycle with the sample under a pressure of 133 MPa.

Figure 2 shows selected x-ray-diffraction patterns measured during the first heating cycle with the sample under a pressure of 133 MPa. At a temperature of 430 K four Bragg peaks are visible in the diffraction pattern recorded for a sample not thermally cycled, whereas at the same temperature under atmospheric pressure the sample is in the isotropic liquid phase. A similar pattern is observed up to about 450 K. Three of the Bragg peaks (signals 1, 2 and 3) correspond to spacings d which are in the ratio 1:2:3, and are associated with a S_{C*2} lamellar structure with periodicity $d_C=42.1$ Å; the fourth one (signal 4) is characteristic of a S_{A*1} structure with layer thickness $d_A=25.2$ Å. Therefore, under these conditions the S_{C*2} and S_{A*1} mesophases coexist, as already observed at ambient pressure in the temperature range between 373 and 406 K [11]. Above a temperature of about 450 K, only the S_{A*1} mesophase is still present, and persists up to about 460 K where finally isotropization occurs. Figure 3 shows the trend of the d spacing of both the bilayer and monolayer smectic mesophases with temperature, in the thermal range covered in the first heating cycle. We observe a temperature dependence much slighter than that measured at atmospheric pressure [11], which is in agreement with the reduced molar volume available at high pressure. The relative contraction $\Delta d/d$ of the layer spacing on passing from atmospheric pressure to 133 MPa is similar for the two mesophases, i.e., $\Delta d/d=6.6\%$ and $\Delta d/d=7.5\%$ for the S_{A*1} and S_{C*2} phases, respectively. This means that the pressure increment has essentially the same effect on the structural reorganization of the macromolecules in the different smectic domains due to the reduced molar volume. However, the higher value of $\Delta d/d$ for the S_{C*2} mesophase reflects the higher layer compressibility of this structure as a consequence of the bilayer interdigitated arrangement [Fig. 1(b)].

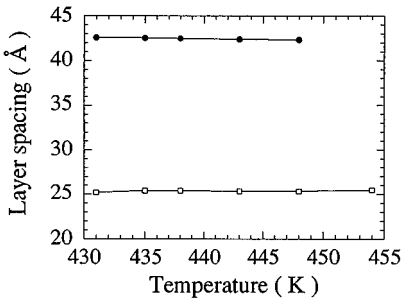

FIG. 3. Temperature dependence of the d spacing of the bilayer smectic-C^* mesophase (full dots) and the monolayer smectic-A^* mesophase (open squares) in the thermal range covered by the first heating cycle.

Figure 4 shows selected x-ray-diffraction patterns measured during the first cooling cycle at 133 MPa. The smectic $A^* \rightarrow$ isotropic phase transition is reversible on cooling, and the S_{A*1} phase appears again below 445 K. The intensity increase of the peak characteristic of the S_{A*1} phase, as the temperature decreases, is shown in the inset of Fig. 4. However, as shown in Fig. 5, a further temperature reduction does not result in the formation of the S_{C*2} mesophase. Crystallization begins instead below 420 K, and is completed at about 390 K, as shown in detail in Fig. 6. The diffractogram of the solid phase is similar to the one of the S_{C*2}, but the positions of the Bragg peaks are no longer in the 1:2:3 ratio.

B. Electron density profile in the S_{C*2} mesophase

The presence of several orders of reflection in the x-ray-diffraction patterns of the S_{C*2} phase means that the projections of the electron density along the normal to the smectic layers cannot be described by an ideal single sinusoidal modulation. Such behavior, already shown at atmospheric pressure, is different from the one of conventional smectic phases encountered in low molar mass systems [20]. The projection of the electron density profile along the normal z to the smectic layers, $\Delta\rho(z)$, in the S_{C*2} phase was calculated as a Fourier sum from the intensity of the Bragg peaks (1, 2, and 3 in Fig. 2),

$$\Delta\rho(z)=\frac{\rho(z)-\langle\rho\rangle}{[\langle\rho^2(z)\rangle-\langle\rho\rangle^2]^{1/2}}=\sum_{\ell=1}^{3} F_\ell \cos\left(2\pi\ell\,\frac{z}{d_C}\right), \tag{1}$$

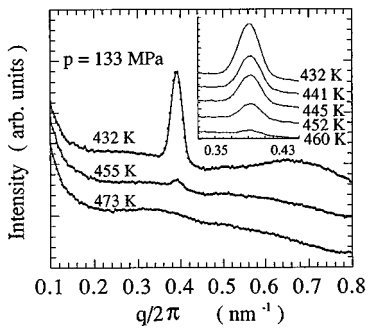

FIG. 4. X-ray-diffraction patterns recorded during the first cooling cycle at $p=133$ MPa. The inset shows the evolution of the intensity of the peak characteristic of the smectic-A^* mesophase.

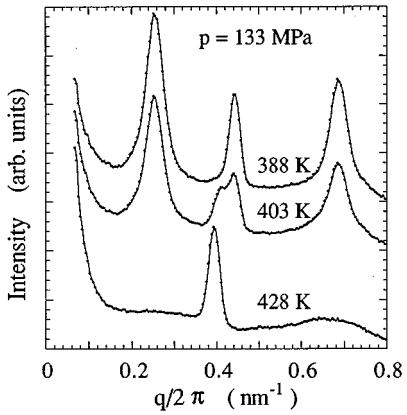

FIG. 5. X-ray-diffraction patterns recorded during the first cooling cycle at $p=133$ MPa, for temperatures between 428 and 388 K. The sample does not exhibit the S_{C*2} structure observed in the first heating cycle, but undergoes a phase transition from the monolayer S_{A*} to the crystalline phases.

where $\rho(z)$ is the electron density, $\langle\rho\rangle$ its average value, F_ℓ is the structure factor of the (00ℓ) reflection, d_c is the layer spacing, and the origin of the z axis is chosen in the middle of the smectic layer. The phase problem was solved by using a pattern recognition approach based on the histogram of the electron density map $\Delta\rho(z)$ [21], following the same steps detailed in Ref. [11]. The results are shown in Fig. 7, where they are compared with the profile at ambient pressure. The two minima of $\Delta\rho(z)$ correspond to the aliphatic spacers, the two principal maxima are associated with the mesogenic cores, and the two secondary maxima at $z=\pm 0.5 d_C$ are due to the polymer backbones. At ambient pressure, the high value of the secondary maxima indicates that the backbones are strongly confined between adjacent sublayers of mesogenic cores, whereas the extension of the principal maxima along z, corresponding approximately to the z projection of the length of the mesogenic cores, indicates only a small expansion due to the translational fluctuations of the chains. Accordingly, at atmospheric pressure the configuration of the side chains does not depart considerably from the full extended one. This situation is modified by applying pressure: the secondary maxima have a smaller relative intensity and a

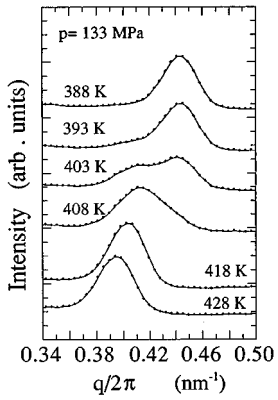

FIG. 6. Temperature evolution of the diffraction intensity in the angular region of the smectic reflection.

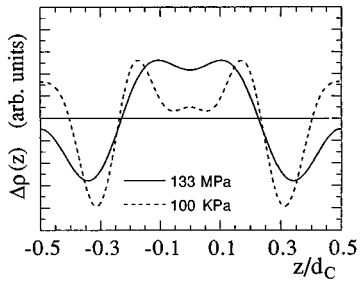

FIG. 7. Electron density profile along the normal to the smectic layers in the smectic-C^* phase, calculated at ambient and high pressure from the intensities of the Bragg peaks.

larger width, revealing a distortion of the backbones. The principal maxima get closer to each other as a consequence of the layer thickness contraction which results in a stronger interdigitation of the terminal substituents. From the position of these maxima, $z=\pm 0.11 d_C$, it is possible to obtain a reliable estimate of the average tilt angle β of the side chains with respect to the layer normal **n**. In fact, if we assume that the main maxima correspond to the position of the centers of the aromatic cores and consider the side chain in the fully extended conformation, an average tilt angle of $\beta=28°\pm 3°$ is found. This value is very close to the one, $\beta=30°$, obtained at atmospheric pressure from the x-ray-diffraction pattern of the oriented mesophase of the fiber sample [11]. The substantial coincidence of these values indicates that the layer compression associated with the pressure increment is absorbed by the sample through a stronger interdigitation of the terminal substituents, without any appreciable modification of the tilt angle β.

Moreover, the broadening of the other features of the electron density profile indicates an increase of the positional disorder inside the smectic layer. This effect is quantitatively estimated by calculating the positional smectic layer order parameters of the positional distribution function of the smectic layers, $f(z)$.

C. Positional smectic order parameters

Following the procedure described is Refs. [22,23], $f(z)$ can be expanded in terms of a Fourier series

$$f(z)=\left(1+\sum_{\ell=1}^{\infty} 2\tau_\ell \cos\left(2\pi\ell\,\frac{z}{d_C}\right)\right)\Big/\, d_C, \qquad (2)$$

where $\tau_\ell=\langle\cos(2\pi\ell z/d_C)\rangle$ is a smectic layer order parameter, which ranges from 1 for the perfect layer structure to 0 for absence of layer structuring. The scattering factor F_ℓ for the scattering vector **q** along the z direction can be written as

$$F_\ell=\sum_m \langle f_m \exp(2\pi i\ell z'_m/d_C)\rangle, \qquad (3)$$

where m denotes the atoms in the molecule, f_m is the atomic form factor of the mth atom, and the average is taken over all molecular configurations. If we indicate by z_{m0} the z coordinates for a perfectly ordered smectic structure ($\tau_\ell=1$), then $z'_m=z_{m0}+z_m$, where z_m gives the fluctuation of the mth atomic position around z_{m0}, and Eq. (3) can be written as

$$F_\ell=\sum_m \langle \exp(2\pi i\ell z_m/d_C)\rangle f_m \exp(2\pi i\ell z_{m0}/d_C). \qquad (4)$$

If z_m is supposed to be the same for all atoms in the molecule, then the intensity I_ℓ of the 00ℓ reflection can be written as

$$I_\ell=C|F_\ell|^2=\tau_\ell^2 I_\ell^0, \qquad (5)$$

where C is a proportionality constant, and I_ℓ^0 is the intensity for a perfectly ordered smectic layer. When more orders of reflection are observed, as it is for polyacrylate 1, then the assumption of a simple model for I_ℓ^0 and a form for $f(z)$ enables us to obtain τ_ℓ. By assuming a Gaussian distribution for $f(z)$ [24],

$$f(z)=[2\pi\langle z^2\rangle]^{-1/2}\exp(-z^2/2\langle z^2\rangle), \qquad (6)$$

the smectic layer order parameters take the form

$$\tau_\ell=\exp(-2\pi^2\ell^2\langle z^2\rangle/d_C^2), \qquad (7)$$

where $\langle z^2\rangle$ is the mean-square displacement of the atoms along the normal to the smectic layers, i.e., the mean-square longitudinal fluctuation of the layers. From Eq. (5) we obtain

$$\frac{I_{\ell+\ell}}{I_\ell}=\frac{\tau_{\ell+1}^2}{\tau_\ell^2}\,\frac{I_{\ell+1}^0}{I_\ell^0}. \qquad (8)$$

The intensity ratios $I_{\ell+1}^0/I_\ell^0$ ($\ell=1,2,\ldots$) can be calculated for a simple model where the side chains assume a planar fully extended conformation, with an average tilt angle of 28° to the layer normal. The values obtained are not very sensitive to the details of the model, especially for the lower values of ℓ. In particular, with $\ell=1$ we obtain $I_2^0/I_1^0=2.05$. The ratio I_2/I_1 is determined from the x-ray-diffraction data, and the value obtained at $T=431$ K is $I_2/I_1=0.21$. With these values for I_2^0/I_1^0 and I_2/I_1, Eq. (8) gives $\tau_2/\tau_1=0.32$. Expressing the ratio τ_2/τ_1 by means of Eq. (7) finally gives the average square fluctuation of the smectic layers $(\langle z^2\rangle)^{1/2}=5.84$ Å. Once we determined $\langle z^2\rangle^{1/2}$, Eq. (7) allows one to calculate the whole set of positional smectic order parameters τ_ℓ. In particular we find $\tau_1=0.68$, $\tau_2=0.22$, and $\tau_3=0.03$ for the first three harmonics of the distribution function. A similar calculation performed for the S_{C*2} mesophase at ambient pressure and temperature $T=363$ K [11] gave a lower value of the average square fluctuations, $\langle z^2\rangle^{1/2}=3.13$ Å, and higher values of the positional smectic order parameters, i.e., $\tau_1=0.91$, $\tau_2=0.69$, $\tau_3=0.43$, $\tau_4=0.22$, and $\tau_5=0.09$ for the five harmonics experimentally observed. The faster decay of τ_ℓ compared to ambient pressure is a consequence of the stronger fluctuations of the layers, in agreement with the expansion of the electron density maxima shown above. However, the stronger thermal fluctuations due to the higher temperatures of the S_{C*2} mesophase stability range at high pressure are not sufficient to account for the observed increment of $\langle z^2\rangle^{1/2}$ with increasing pressure. In fact, according to the model of de Gennes and Prost [20], the mean-square fluctuation in a smectic liquid crystal can be written as

$$\langle z^2\rangle = \frac{k_B T}{4\pi\lambda B}\ln\left(\frac{L}{d}\right), \tag{9}$$

where k_B is the Boltzmann constant, T is the absolute temperature, L is the linear size of the smectic domain, d is the layer spacing, B is the elastic constant for compression, and λ is a characteristic length of the material of the order of the layer thickness. In practice, a simple proportionality relation between $\langle z^2\rangle$ and T holds if we consider that the constants in Eq. (9) are only slightly temperature dependent (especially far from the smectic to isotropic phase transition). This temperature scaling law was experimentally verified for the sample at ambient pressure, by comparing the values of $\langle z^2\rangle$ calculated at room temperature and at $T=363$ K. From Eq. (9), we obtain $\langle z^2\rangle|_{T=431}=(431/363)\langle z^2\rangle|_{T=363}$, i.e., $\langle z^2\rangle^{1/2}=3.41$ Å. Accordingly, the remaining difference between this value and the one measured at $p=133$ MPa, $\langle z^2\rangle^{1/2}=5.84$ Å, is a direct consequence of the pressure effects on the structural properties of the mesophase, and can be explained in terms of the induced static positional disorder of the smectic layers as a consequence of the reduced molar volume. If we neglect, to a first approximation, the pressure dependence of the constants B, L, and d in Eq. (9), and assume a Gaussian distribution function for the static disorder [25], we can write the mean-square fluctuation $\langle z^2\rangle$ as the sum of two contributions

$$\langle z^2\rangle = \langle z^2\rangle_T + \langle z^2\rangle_D, \tag{10}$$

where the first term represents the thermal contribution [Eq. (9)], and the second one is the mean-square fluctuation of the layers due to the static positional disorder. From the knowledge of $\langle z^2\rangle^{1/2}=5.84$ Å and $\langle z^2\rangle_T^{1/2}=3.41$ Å, the value $\langle z^2\rangle_D^{1/2}=4.74$ Å can be estimated by means of Eq. (10). This result shows that the effect of the static positional disorder, which is negligible at atmospheric pressure, at high pressure is of the same order as that due to the thermal fluctuations.

A more accurate evaluation of $\langle z^2\rangle_D$ should take into account the pressure dependence of $\langle z^2\rangle_T$, i.e., the variation of the quantities B, L, and d in Eq. (9) with pressure. A reliable estimate of L can be obtained by means of the Scherrer formula [26]

$$L = \frac{0.9}{\Delta(q/2\pi)}, \tag{11}$$

where $\Delta(q/2\pi)$ is the full width at half maximum (FWHM) of the Bragg peaks in the I vs $q/2\pi$ experimental curve (Fig. 2). The values obtained for $\Delta(q/2\pi)$, after deconvolution of the Bragg peaks for the instrumental resolution function, are 4.1×10^{-3} Å^{-1} (at atmospheric pressure) and 7.9×10^{-4} Å^{-1} (at $p=133$ MPa) which correspond to $L\approx1140$ and 220 Å, respectively. In addition, d varies from ≈46 Å, at atmospheric pressure, to ≈42 Å, at $p=133$ MPa. Therefore both quantities, L and d, reduce with increasing pressure. However, the reduction of d being rather small and the dependence on L/d relatively weak [see Eq. (9)], this effect does not seem to play a critical role in the above calculation of the static positional disorder. Concerning the elastic constant B, experimental values are not known, and no theoretical model is presently available for its pressure dependence.

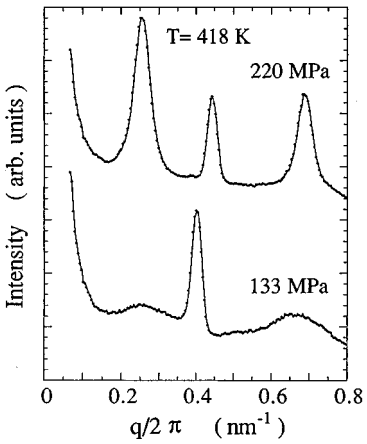

FIG. 8. Diffraction patterns recorded at 418 K at 133 and 220 MPa.

However, we should expect that a pressure increase results in a higher layer rigidity for compression and, therefore, in higher values of B. According to these considerations, any pressure increment acts in the sense of reducing $\langle z^2\rangle$ differently from what was experimentally observed. This result supports our interpretation of the pressure-induced increment of $\langle z^2\rangle$ as an effect of the increment of the static positional disorder, even though, to account for the unknown pressure dependence of B, the value $\langle z^2\rangle_D=4.74$ Å must be considered as a lower limit for the static positional disorder.

D. Mesomorphic behavior at 220 MPa

After reaching the minimum temperature, $T=363$ K, in the cooling cycle at $p=133$ MPa, a further increase of pressure up to 220 MPa does not modify the crystal habit of the sample, but only produces a contraction of the crystallographic cell, as revealed by the shift of the Bragg peaks. However, the range of stability of the crystal phase is extended to higher temperatures. In fact, as shown in Fig. 8, at $T=418$ K and $p=220$ MPa, the system is still in the crystalline phase, whereas at the same temperature and $p=133$ MPa the smectic-A^* order is dominant. At higher temperatures, a peak corresponding to a periodicity of $d=25$ Å appears in the diffraction pattern at $T=428$ K, indicating the beginning of a transition toward a S_{A*1} phase which is completed only at 463 K (Fig. 9). The range of this transition is unusually large even for a polymeric liquid crystal, and reflects the

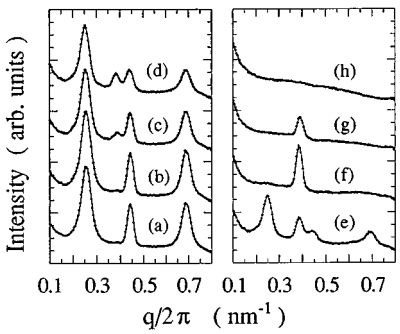

FIG. 9. Temperature evolution of the diffractograms recorded during the heating cycle at 220 MPa. (a) 419 K, (b) 423 K, (c) 437 K, (d) 447 K, (e) 456 K, (f) 463 K, (g) 473 K, and (h) 493 K.

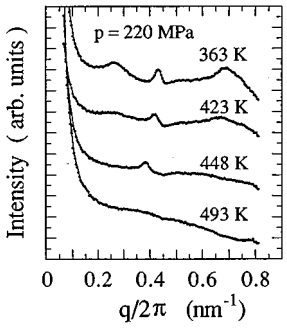

FIG. 10. Diffraction patterns obtained on cooling from the isotropic melt, with the sample under a pressure of 220 MPa.

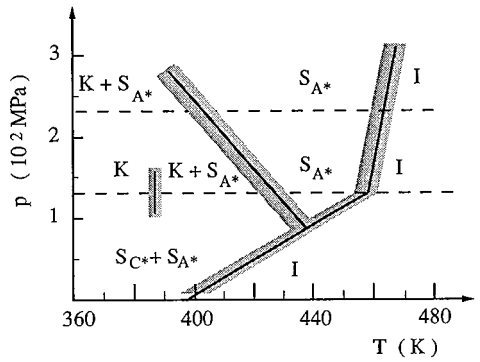

FIG. 11. Proposed pressure-temperature phase diagram for the investigated polymer. The symbols refer to the isotropic melt (I) and monolayer smectic-A^* (S_{A*}), the smectic-C^* (S_{C*}), and crystalline (K) phases. The broken lines show the pathways along which measurements have been carried out. The shadowed regions indicate the uncertainties on the phase boundaries.

reduced mobility which follows the molar volume contraction. The S_{A*1} phase is stable up to 493 K, where isotropization occurs.

By cooling down isobarically from the isotropic melt (Fig. 10), the S_{A*1} phase is regained at about 460 K, and remains stable down to about 400 K, where a short-range crystalline order starts to develop, as revealed by the appearance of broad and diffuse diffraction peaks. The effect of the pressure p on the smectic long-range positional order can be determined by considering the behavior of the longitudinal correlation length in the S_{A*1} mesophase, $\xi_{\parallel}$, when p is raised from ambient pressure up to 220 MPa. The correlation length is calculated as

$$\xi_{\parallel}=\frac{2}{\Delta q}, \tag{12}$$

where Δq is the FWHM of the Lorentzian curve describing the shape of the diffraction peak in the experimental pattern deconvoluted for the instrumental resolution function. The values obtained are $\xi_{\parallel}\approx 400$ Å, at ambient pressure, and $\xi_{\parallel}\approx 100$ Å at pressures higher than 133 MPa. The reduction of the correlation length with increasing pressure up to 133 MPa is in agreement with the measured increment of the static positional disorder. The constant value of $\xi_{\parallel}$ observed above 133 MPa clearly indicates a saturation which is reached as a consequence of the minimization of the molar volume (compatible with the steric packing requirements). This is also confirmed by the constancy of the layer spacing above 133 MPa.

On the basis of the observations described, the schematic pressure-temperature phase diagram shown in Fig. 11 has been deduced. It refers to the behavior of the system when the temperature is lowered isobarically from high to room temperature. Of course, the boundaries must be considered only as tentative lines interpolating the experimental data. An increase of the clearing point with the pressure is evident, but the most salient feature is the stabilization of the smectic-A^* phase for $p>100$ MPa. The interval over which the polymer exhibits the S_{A*1} structure becomes progressively larger as pressure increases, mainly because the transition to the solid phase shifts toward lower temperatures. This finding suggests that a further increase of pressure could result in the extension of the smectic-A^* order down to room temperature. Moreover, if the proposed phase boundaries are correct, an isothermal increase of pressure at temperatures around 420 K should result in a reversible isotropic → crystalline → smectic transformation sequence, which appears to be an unusual behavior.

IV. CONCLUSIONS

The phase behavior of a chiral side-chain polyacrylate has been observed upon increasing pressure up to 220 MPa by *in situ* x-ray diffraction. The modifications of the macromolecular organization in the S_{C*2} mesophase have been discussed in terms of the electron density profile along the normal to the smectic layers. The pressure effects on the smectic ordering have been quantitatively estimated by calculating the variation of the positional smectic order parameters and the longitudinal correlation lengths. The stabilization of the smectic-A^* phase at high pressure has been shown. This could play a significant role in technological applications of chiral liquid crystals for electro-optical devices and components.

ACKNOWLEDGMENTS

It is a pleasure to thank Professor E. Chiellini and Professor G. Galli, of the University of Pisa, Italy, who provided the samples used in this investigation.

[1] K. Kondo, S. Eera, M. Isogai, and A. Mukoh, Jpn. J. Appl. Phys. **24**, 1389 (1985).
[2] G. Decobert and J. C. Dubois, Mol. Cryst. Liq. Cryst. **144**, 199 (1987).
[3] J. W. Goodby, M. A. Waugh, S. M. Stein, E. Chin, R. Pindak, and J. S. Patel, Nature (London) **339**, 449 (1989).
[4] G. Scherowsky and M. Sefkov, Liq. Cryst. **12**, 355 (1992).
[5] L. Komitov, S. T. Lagerwall, B. Stebler, E. Chiellini, G. Galli, and E. Dossi (unpublished).
[6] S. Garoff and R. B. Meyer, Phys. Rev. Lett. **38**, 848 (1977); Phys. Rev. A **19**, 338 (1979).
[7] N. A. Clark and S. T. Lagerwall, Ferroelectrics **58**, 215 (1984).

[8] G. Andersson, I. Dahl, P. Keller, W. Kuczynski, S. T. Lagerwall, K. Skarp, and B. Stebler, Appl. Phys. Lett. **51**, 640 (1987).
[9] G. Andersson, I. Dahl, W. Kuczynski, S. T. Lagerwall, K. Skarp, and B. Stebler, Ferroelectrics **84**, 285 (1988).
[10] E. Chiellini, G. Galli, F. Cioni, E. Dossi, and B. Gallot, J. Mater. Chem. **3**, 1065 (1993).
[11] O. Francescangeli, D. Rinaldi, M. Laus, G. Galli, and B. Gallot, J. Phys. (France) II **6**, 77 (1996).
[12] M. Laus, A. S. Angeloni, G. Galli, and E. Chiellini, Termochim. Acta **227**, 49 (1993).
[13] E. Chiellini, G. Galli, F. Cioni, E. Dossi, and B. Gallot, J. Mater. Chem. **3**, 1065 (1993).
[14] R. Caciuffo, O. Francescangeli, B. Paci, P. Bösecke, C. Ferrero, and M. Lorenzen, Europhys. Lett. **34**, 501 (1996).
[15] Y. Maeda and J. Watanabe, Macromolecules **28**, 1661 (1995).
[16] Y. Maeda, N. Tanigaki, and A. Blumstein, Mol. Cryst. Liq. Cryst. **227**, 407 (1993).
[17] S. Rastogi, M. Newman, and A. Keller, J. Polym. Sci. Polym. Phys. **31**, 125 (1993).
[18] S. Rastogi, M. Newman, and A. Keller, Nature **353**, 55 (1991).
[19] P. Bösecke, O. Diat, and B. Rasmussen, Rev. Sci. Instrum. **66**, 1636 (1995).
[20] P. G. De Gennes and J. Prost, *The Physics of Liquid Crystals* (Oxford University Press, Oxford, 1993).
[21] V. Luzzati, P. Mariani, and H. Delacroix, Macromol. Chem. Macromol. Symp. **15**, 1 (1988).
[22] P. J. Wojtowicz, in *Introduction to Liquid Crystals*, edited by E. B. Priestley, P. J. Mojtowicz, and P. Sheng (Plenum, New York, 1974).
[23] A. J. Leadbetter, in *The Molecular Physics of Liquid Crystals*, edited by G. R. Luckhurst and G. W. Gray (Academic, London, 1979).
[24] A. J. Leadbetter, J. C. Frost, J. P. Caughan, G. W. Gray, and A. J. Mosley, J. Phys. (Paris) **40**, 669 (1979).
[25] R. Hosemann and S. N. Bagchi, *Direct Analysis of Diffraction by Matter* (North-Holland, Amsterdam, 1962).
[26] B. D. Cullity, *Elements of X-Ray Diffraction* (Addison-Wesley, Reading, MA, 1978).